Molecular conductance

Valkenier-van Dijk, Elisabeth Hendrica

Chapter 7
The Matrix Approach Revisited

In this concluding chapter we summarize and discuss the results from the Matrix Approach, in which the conductance of several series of molecular wires was investigated by five methods. We describe the trends in the molecular conductance that we found for these series and how the junction geometry influences these trends and the absolute conductance values. Additionally, we compare the results from conductance measurements on monothiolated and dithiolated molecular wires in different junctions. We finish this chapter with a discussion on the consequences of the results of our conductance studies.

7.1 Results from the Matrix Approach

In Chapter 1.5 we have introduced our Matrix Approach on molecular conductance. We have designed and synthesized five series of molecular wires (described in the Chapters 2, 3, 4, and 6), that all have their rigid oligo(1,4-phenylene ethynylene) (OPE)-based structure and thiolate anchoring groups in common. We varied the length, HOMO-LUMO gap and conjugation pattern of these wires by changing their central unit, to study the influence of these properties on the conductance. In collaborations with different groups, we have used several methods to study the conductance of these wires. These are single molecule methods like Scanning Tunneling Microscopy Break Junctions (STM-BJ) and Mechanically Controllable Break Junctions (MCBJ), Conductive Probe Atomic Force Microscopy (CP-AFM, by which about a hundred molecules are contacted), and much larger junctions formed with the eutectic alloy of gallium and indium as top contact (EGaIn) as well as Large Area Molecular Junction (LAMJ) devices. Before we present the overview of the results obtained by this Matrix Approach and the conclusions in Section 7.1.3, we present the results from CP-AFM and MCBJ studies on the length dependence of the conductance OPEs in the next two sections.

7.1.1 OPE Length Dependence of the Conductance in CP-AFM junctions[1]

We have grown SAMs of molecular wires **OPE2-4** according to the triethylamine deprotection procedure described in Chapter 3 and investigated the charge transport through these SAMs upon contacting with a gold-coated contact-mode AFM tip as described in Chapter 5.3. *I-V* curves were measured and conductances were obtained from linear fits of the data between -100 mV and 100 mV. Histograms from these conductances are given in Figure 7.1a. We obtained a conductance value for each OPE from a Gaussian fit of the largest peaks in the histogram. A semilogarithmic plot of these values versus the molecular length shows that the conductance (G) decays exponentially with the length (L), according $G = A \cdot e^{-\beta L}$ with exponential decay parameter $\beta = 0.37$ Å^{-1} (Figure 7.1b). This is in very good agreement with the value $\beta = 0.33$ Å^{-1} that we found for **OPE2-4** in the STM Break-Junction method (Chapter 4) and with the value reported for electrochemical charge transfer experiments through OPE bridges

(0.36 Å^{-1}),[2] though larger than the values previously reported for CP-AFM experiments with Ti/Pt tips (0.21 Å^{-1})[3] and on OPEs with amine anchoring groups (0.20 Å^{-1}).[4]

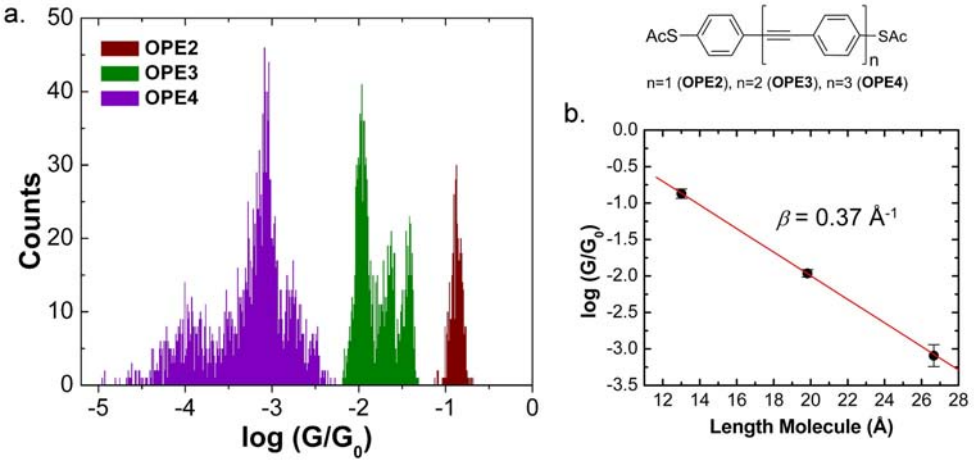

Figure 7.1 a. Conductance histograms of **OPE2-4** obtained from CP-AFM measurements. **b.** Fit of the exponential decay of the conductance of **OPE2-4** as function of the molecular length with β = 0.37 Å^{-1}. (*Leiden*, note 1)

7.1.2 OPE Length Dependence of the Conductance in MCBJs[5]

The conductance of **OPE2-4** was investigated by Wenjing Hong, University of Bern, with notched gold wire-based MCBJs. The wire was broken in the presence of a 0.1 mM solution of bisacetyl protected OPE dithiols in mesitylene/THF (4:1) on air. The break junction was repeatedly opened and closed, while measuring conductance-distance traces. The resulting histograms are depicted in Figure 7.2a and the positions of the peaks are very close to those found in the STM-BJ experiments (see also Table 7.1). The fit of these conductance values gave an exponential decay parameter β = 0.34 Å^{-1}, being very close to the values found by STM-BJ (0.33 Å^{-1}) and CP-AFM (0.37 Å^{-1}).

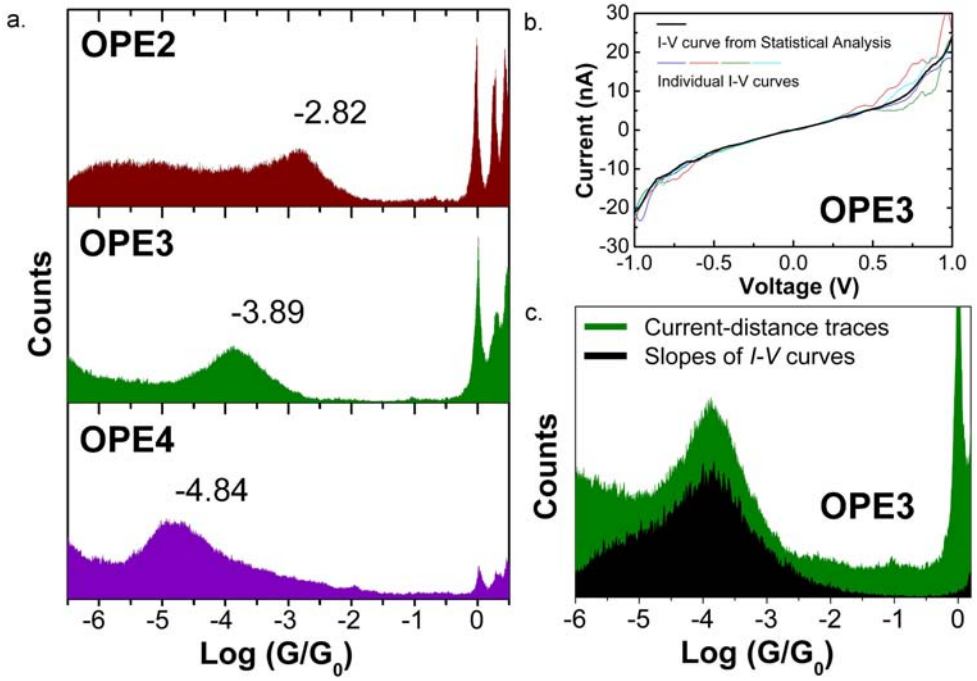

Figure 7.2 Results from conductance measurements in notched gold wire-based mechanically controllable break junctions (ambient) at a bias of 100 mV. **a.** Histograms from conductance-distance traces of **OPE2-4**. **b.** I-V curves of **OPE3**. **c.** Conductance histogram of **OPE3** obtained from a linear fit (-0.5 to 0.5 V) of the slope of 16575 individual I-V curves (black), which shows a peak at the same position as the conductance histogram that was obtained from 1600 conductance-distance traces (green). (*Bern*, note 5)

I-V curves were recorded while slowly opening and closing the junction with **OPE3**.[6] The mean curve from the statistical analysis is plotted in Figure 7.2b, together with a few individual *I-V* curves. The slope of the linear regime (-500 mV to 500 mV) was determined for all individual *I-V* curves and a histogram was constructed from the obtained conductance values (Figure 7.2c, black), which has a shape similar to the histogram from the conductance-distance traces (Figure 7.2c, green). This confirms that the conductance values that are obtained from current-distance traces in break junction experiments (STM-BJ and MCBJ) can be compared directly to conductance values determined from *I-V* curves (as in this MCBJ experiment, but also in CP-AFM experiments). This supports the good agreement found between the conductance values obtained from CP-AFM measurements and from break junction methods (Figure 7.3).

7.1.3 The Matrix Approach: Summary and Conclusions

The Matrix Approach offers the advantage that all molecules have an identical design (an OPE-type core and two thiolate anchoring groups) and that all molecules, of which the conductance was measured in different laboratories, were synthesized in the same laboratory according to a general strategy. Furthermore, the formation of unreproducible or ill-defined self-assembled monolayers (SAMs) was excluded by an in depth investigation of the self-assembly (Chapter 3).

The results of these investigations are summarized in Table 7.1 and Figure 7.3. To estimate the conductance per molecule we assumed that around a hundred molecules are contacted in the CP-AFM junction[7] and that the packing density of the molecular wires in the SAMs is $4 \cdot 10^{18}/m^2$ (or: $4 \cdot 10^6/\mu m^2$), corresponding to an area of 25 $Å^2$ per molecule.[8]

Not all molecular wires were studied by all possible methods, mainly due to large time consumption and/or high costs of the measurements or practical problems like the high or low current limits of the measurements or problems with the experimental protocols to apply the molecules in the junction. Furthermore, not all methods are suitable to study all series. Molecular wires **4.4** and **4.5,** for instance, are expected to have a packing density that deviates substantially from that of **OPE3**,[9] which obfuscates the comparison of conductance measurements on densely packed SAMs of these molecules.

Comparison of the Methods for Conductance Measurements

When comparing the five different junctions used to study molecular conductance, we find a very good agreement between the results from single molecule STM-BJ and MCBJ experiments and from the measurements on SAMs by CP-AFM (Figure 7.3, upper part). The trends found are identical, as are the absolute conductance per molecule values, based on the assumption that we contact a hundred molecules in a CP-AFM junction. These three methods have in common that gold-molecule-gold junctions are formed, which is a relatively well-defined system. STM-BJ experiments have the advantages to be very fast and not to require densely packed SAMs. MCBJs are more stable compared to STM-BJs, which allows to measure *I-V* curves. An additional advantage is that only a few molecules need to be present on the gold surface of the junction area. In contrast, CP-AFM studies require densely packed SAMs. Since many molecules are measured in parallel, the currents through these junctions are larger and less specialized

electronics can be used. Furthermore, the large number of molecules and the less dynamic character of the junction cancel out small differences in binding geometry. The good agreement between the results from different junctions and different labs shows that these three gold-molecule-gold methods are highly suitable to study the influence of molecular structure on the conductance.

Table 7.1 Summary of the results from the conductance measurements by various methods.

Structure	Name	STM-BJ G (nS)	MCBJ G (nS)	CP-AFM G (nS)	EGaIn G (nS/μm^2)	LAMJ G (nS/μm^2)	Model[a] G (nS)
	OPE2 **4.1**	114	117	10428	-	11749[b]	114
	OPE3 **4.2**	13.9	10.0	841	-	5012[b]	11
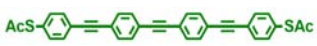	OPE4 **4.3**	1.22	1.1	63	-	4266[b]	1.1
$G = A \cdot e^{-\beta \cdot L}$	β (Å^{-1})	*0.33*	*0.34*	*0.37*	-	*0.07-0.15*[d]	
	**4.4**	20.8	-	-	-	-	15
	**4.5**	36.4	-	-	-	-	43
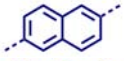	**4.6**	4.12	-	-	-	-	5.8
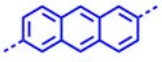	26AC **2.6/4.7**	3.61	1.95	221	108[e]	15286[c]	4.1
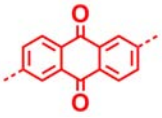	AQ **2.1**	-	0.008	6.9	0.69[e]	5750[c]	1.1
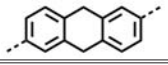	H2AC **2.7**	-	0.04	32	1.9[e]	2512[c]	2.3

a. Predicted values for tunneling through a rectangular barrier, based on the length and HOMO level (see Chapter 4.5). The results from STM-BJ experiments are used to parameterize this model.

b. Devices were fabricated at MiPlaza in Eindhoven, according ref. 10 and the resistance was determined at 0.5 V.

c. Devices were fabricated at the University of Groningen (see Section 5.9.2) and the resistance was determined at 0.1 V.

d. The series [benzenedithiol-OPE2-OPE3] gave a β value of 0.15 Å^{-1}, whereas the series [OPE2-OPE3-OPE4] gave a β value of 0.07 Å^{-1}.

e. Determined from a Gaussian fit of the current density histogram at 0.1 V.

* All conductance measurements are performed in collaborations, as listed in Chapter 1.5.

The molecular conductance values obtained from LAMJ and EGaIn experiments are four to five orders of magnitude lower (Figure 7.3, gray background). We might have overestimated the packing density of the molecules or the contact area (due to trenches in the gold surface, in which the molecules are not contacted by the top electrode, or due to defects in the SAM), though these parameters will count for one to two orders of magnitude at most. A better explanation for these orders of magnitude lower conductances is found in the top contacts. The resistance of the ~90 nm thick PEDOT:PSS interlayer and its interface with the SAM contribute ($r_{SAM/PEDOT:PSS}$) to the total resistance of the LAMJ (R_{LAMJ}) in a factorized way ($R_{LAMJ} = 12.9\ k\Omega \cdot r_{Au\text{-}S} \cdot r_{SAM} \cdot r_{SAM/PEDOT:PSS}$).[7] In EGaIn junctions the SAM is separated from the metallic GaIn top contact by a thin layer of Ga_2O_3 (~1 nm), which most likely acts as an additional tunneling barrier. These more

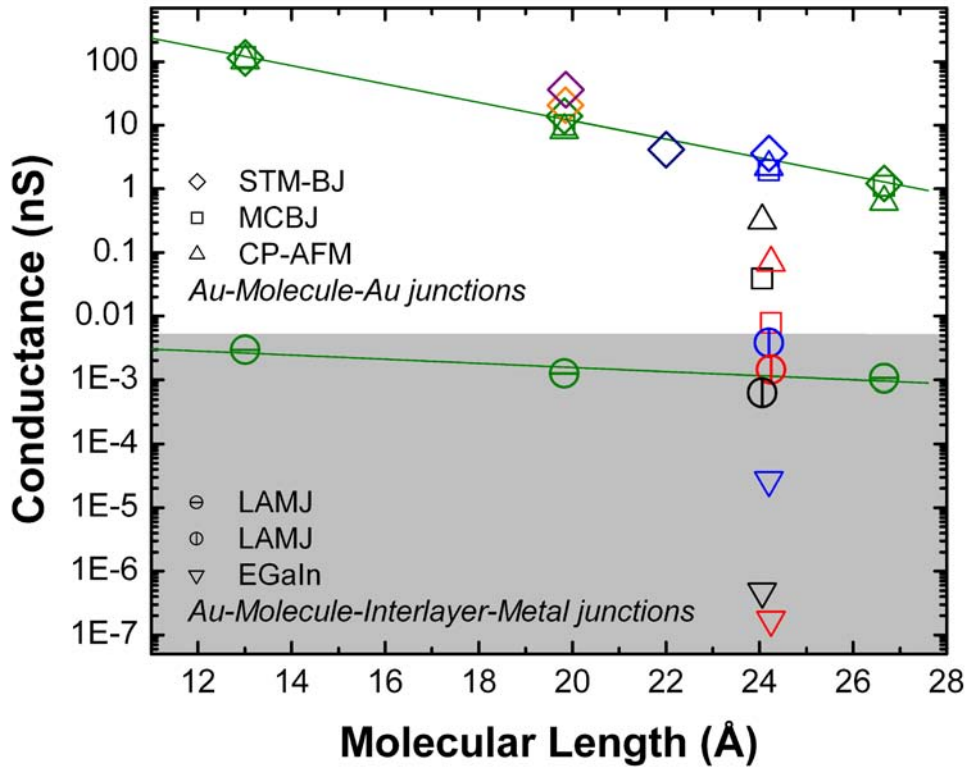

Figure 7.3 Results of the Matrix Approach: Plot of the low bias conductance per molecule versus the length of the molecular wires for wires **OPE2-4** (green), **4.4** (orange), **4.5** (purple), **4.6** (dark blue), **4.7**=**26AC** (blue), **AQ** (red), **H2AC** (black). The results from different methods are plotted with different symbols. Exponential fits of the STM-BJ data and LAMJ data on **OPE2-4** are plotted as green lines. The upper part of this plot contains all values measured in junctions with two gold contacts (white background). The lower part of this plot contains the values obtained from junctions with a top contact other than gold (gray background).

complex top contacts of LAMJs and EGaIn junctions not only give rise to lower absolute conductance values, but also to less strong length dependence of the conductance (*i. e.*, lower values for exponential decay parameter β). A difference between these two methods is the large influence of the conjugation pattern on the conductance found in EGaIn junctions, compared to the less pronounced trend in LAMJs.

EGaIn junctions, LAMJs and junctions formed by CP-AFM have the requirement of high quality densely packed SAMs in common. An advantage of EGaIn junctions and LAMJs is that these junctions are formed over areas of around 80-8000 μm^2, which provides the possibility to study the influence of the quality of the SAM on the charge transport properties, as is possible with mercury junctions.[11] In Chapter 3.6 we have shown that the conditions used for the formation of SAMs determine the resistance of LAMJs up to three orders of magnitude. When using EGaIn as a top contact, the yield of good junctions decreases dramatically when SAMs are less densely packed, leading to a large percentage of shorted junctions.[12]

The trends found in the absolute conductance values upon comparing different types of junctions with π-conjugated wires are in good agreement with the trends described for alkanethiol junctions formed by different methods[13]: we found the highest conductance values (or lowest resistance) when the molecules had two chemisorbed contacts (*e.g.*, thiolate-gold bonds in STM-BJ, MCBJ, CP-AFM), lower conductance values for molecules with one chemisorbed contact (see Section 7.2.1), and the lowest conductance values in the presence of a resistive interlayer (PEDOT:PSS in LAMJs or Ga_2O_3 in EGaIn junctions). However, in contrast to junctions with alkanethiols, the exponential decay factor β was influenced by the resistive interlayer as well.

Trends in the Relationship between Molecular Conductance and Structure

Figure 7.3 shows a strong dependence of conductance on the molecular length, as described for the STM-BJ results in Chapter 4 and confirmed with the results from CP-AFM and MCBJ measurements (see next sections). The conductance values (G) from these experiments decay exponentially as function of the length (L), according to the description for tunneling through a rectangular barrier: $G = A \cdot e^{-\beta L}$, with exponential decay parameter β varying from 0.33-0.37 $Å^{-1}$. The conductance values from linear conjugated anthracene- and naphthalene-based wires are found

to be very close to the fit belonging to the length dependence of **OPE2-4**. Naphthalene- and anthracene-based wires **4.4** and **4.5** were found to have 1.5 and 2.6 times larger conductance values than **OPE3**. We attributed this to the relatively high energy of the HOMO levels of these compounds, which decreases the offset between the Fermi energy of the gold electrode and the HOMO, decreasing the height of the tunneling barrier. In the last column of Table 7.1 we listed the values obtained from a highly simplified model for molecular conductance as tunneling through a rectangular barrier in which the width of the barrier is determined by the length of the molecule and the height of the barrier by the offset between the HOMO level and the Fermi energy of gold.[14] Alternative explanations for the relatively large conductance values for these anthracene and naphthalene wires, like their relatively small HOMO-LUMO gap or the gain in aromaticity upon formation of quinoid structures,[15,16] can be traced back to the high energy of the HOMO levels.

Strong deviations from the length dependence trend were found for the cross-conjugated anthraquinone wire (**AQ**, red) and the dihydroanthracene wire with broken conjugation (**H2AC**, black). Their relatively low HOMO levels can only account for a factor two to four reduced conductance and not for the about two orders of magnitude that we found experimentally. We explained the low conductance of the broken-conjugated wires by the lower electronic coupling between their two π-conjugated parts. Also in the cross-conjugated wires the electronic coupling is lower than in linear conjugated wires. Destructive quantum interference was predicted for this cross-conjugated **AQ** wires. This dramatically reduces their conductance at small bias voltages (see Chapter 5).

7.2 A Comparison of the Conductance of Monothiolated and Dithiolated OPE3

In the previous section we have discussed the results from conductance studies on molecular wires with two thiol-based anchoring groups. In this Section we will focus on the comparison of the results from conductance measurements on monothiolated OPE3 (**monoS-OPE3**) and dithiolated OPE3 (**diS-OPE3**), of which the synthesis and formation of self-assembled monolayers were described in Chapter 3.

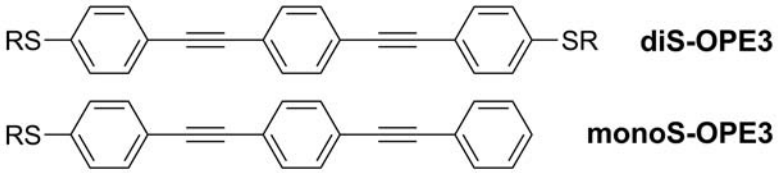

Figure 7.4 Chemical structures of **diS-OPE3** and **monoS-OPE3**.

7.2.1 Comparison of OPE3 monothiol and dithiol in CP-AFM junctions[1]

As we described in Section 7.1, the CP-AFM method does provide relatively well-defined gold-molecule-gold junctions. In these junctions, one thiolate anchoring group is chemisorbed at the gold surface of the substrate, providing a good coupling to the bottom contact. The nature of the top contact could vary. When a SAM of dithiols is contacted, the thiol groups on top of the SAM (about half of

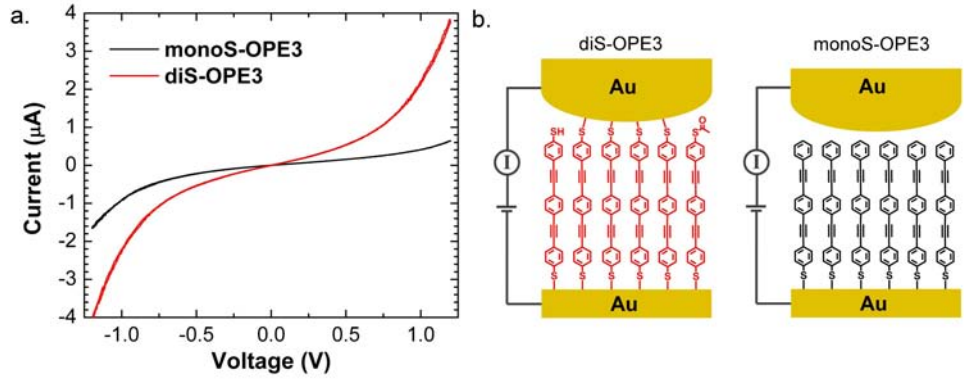

Figure 7.5 Averaged I-V curves of **monoS-OPE3** (black) and **diS-OPE3** (red) as measured by CP-AFM. (*Leiden*, note 1)

which bears an acetyl protecting group) will chemisorb to the gold-coated AFM tip [17] and form a symmetric gold-molecule-gold junction. In contrast, when the AFM tip contacts a SAM of monothiols, then only a physical contact can be formed due to the force on the tip.

We have investigated the conductance of SAMs of **diS-OPE3** and **monoS-OPE3** and plotted the averaged I-V curves in Figure 7.5. We found the I-V curve of **diS-OPE3** to be symmetric, which indicates that indeed a chemisorbed contact between the SAM and gold coated AFM tip was established. In contrast, the I-V curve of **monoS-OPE3** is asymmetric: the current at -1.2 V is 2.5 times larger than the current at +1.2 V. Furthermore, the conductance of **diS-OPE3** at low bias voltages (±100 mV) is around three times larger than the conductance of **monoS-OPE3**, as expected for a junction with one chemisorbed and one physisorbed contact.

7.2.2 Comparison of OPE3 monothiol and dithiol in MCBJs[18]

The conductance of **diS-OPE3** and **monoS-OPE3** was studied in lithographically defined break junctions in vacuum at Delft University.[18] The molecules were applied by immersion of the break junction substrates overnight in solutions of the acetyl-protected molecules in THF (under nitrogen), after which the samples were rinsed, dried and mounted in the setup.[19] Current-distance traces were measured upon opening of the break junctions and histograms were constructed without any data selection. The histogram of **diS-OPE3** as shown in Figure 7.6 shows a broad molecular feature around 10^{-4} G_0, which is not present in the histogram of clean

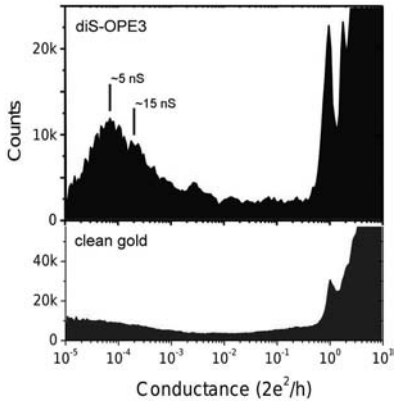

Figure 7.6 Histograms of the conductance-distance traces measured for **diS-OPE3** (blue, 500 traces) and clean gold (red, 2100 traces) in lithographically defined mechanically controllable break junctions in vacuum at a bias of 50 mV and a stretching speed of 1 nm/s. (*Delft*/*Leiden*, note 18)

gold. A clear feature is observed at $7 \cdot 10^{-5}$ G_0 (~5 nS) and a shoulder could be present at $2 \cdot 10^{-4}$ G_0 (~15 nS), though no firm conclusions can be made on that. These values are close to the values obtained from STM-BJ measurements (14 nS) and ambient MCBJ measurements (10 nS) and the values reported in the literature (13 nS,[20] 9 nS,[21] 10 nS,[22] 4 nS[23]).

Two dimensional histograms[24] were obtained for **monoS-OPE3** and **diS-OPE3** (Figure 7.7). The 2D-histogram of **diS-OPE3** shows plateau-like features around 10^{-4} G_0, which have formed the peak in the histogram in Figure 7.6. In contrast, no plateau-like feature are observed for **monoS-OPE3**, indicating that no molecular Au-molecule-Au junctions are formed with this asymmetric molecule, as expected for a molecule with only one anchoring group.

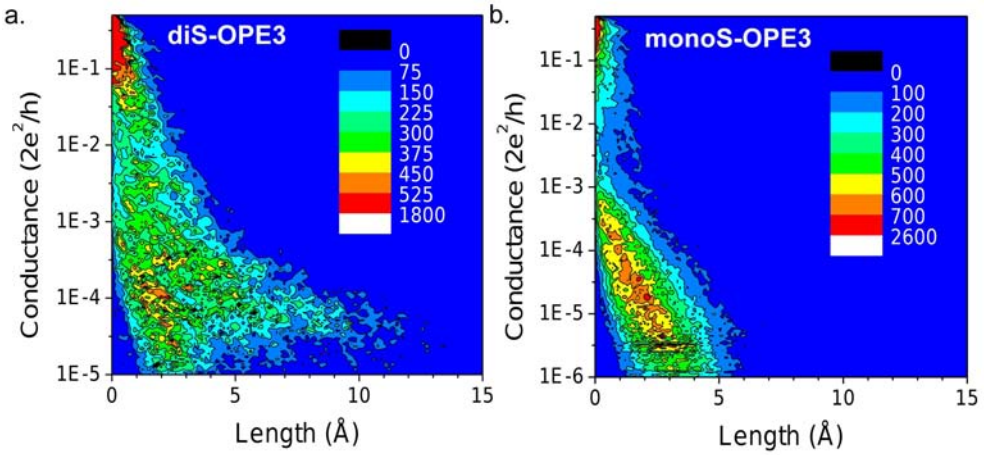

Figure 7.7 2D Histograms of the conductance-distance traces measured for **diS-OPE3** (**a**, 500 traces) and **monoS-OPE3** (**b**, 1600 traces) in lithographically defined mechanically controllable break junctions in vacuum at a bias of 50 mV and a stretching speed of 1 nm/s. (*Delft*/*Leiden*, note 18)

7.2.3 Comparison of OPE3 monothiol and dithiol in STM-BJs[25]

In the discussed MCBJ experiments in vacuum, no conductance was found for monoS-OPE3. However, conductance peaks around $6 \cdot 10^{-6}$ G0 (0.5 nS) were recently recorded in MCBJ experiments in a liquid environment[26] and ambient STM-BJ experiments[27] on this monothiol and on a monoS-OPE3 with two methoxy groups on the central phenyl ring. This low conductance feature was attributed to π-π interactions[28] between two monoS-OPE molecules, each of which is bound to one of the electrodes (Figure 7.8a). A surprisingly large conductance

through π-π stacked conjugated units was previously reported by Seferos et al. for an OPV-type molecular wire of which the two π-conjugated parts were covalently linked in the π-π stacked configuration by a [2,2]paracyclophane unit (Figure 7.8b).[29]

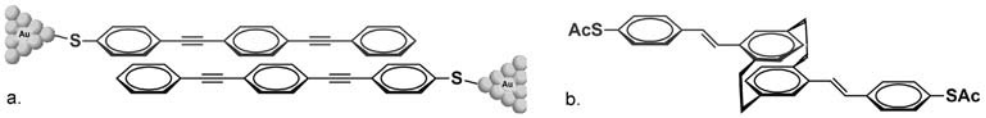

Figure 7.8 a. Schematic of the π-π stacking of two **monoS-OPE3** molecules in a junction (the exact geometry of this stacking phenomenon is unknown). **b.** The covalently bound π-π stacked wire of Seferos *et al*.[29]

To investigate if the reported low conductance feature[26,27] indeed originates from π-π stacking, this interaction was tuned by varying the solvents in the liquid cell of the STM-BJ setup. These experiments were performed by Veerabhadrarao Kaliginedi at the University of Bern. The MCBJ experiments from the Schönenberger group (University of Basel) were performed in mesitylene/THF (4:1),[26] also used in the STM-BJ experiments in Chapter 4. THF was used as a good solvent for the OPE compounds and mesitylene is a high boiling and apolar solvent, which minimizes leakage currents. However, mesitylene is an aromatic solvent which has π-π interactions with the OPE molecules. Better π-π stacking of the monoS-OPE3 molecules in the junctions was therefore expected in a non aromatic solvent like decane. The conductance measurements of diS-OPE3 in decane/THF (5:1) gave a conductance histogram with a large high conductance peak (~19 nS) and a low conductance peak (~0.8 nS, Figure 7.9a), similar to the measurements in mesitylene/THF (Chapter 4). MonoS-OPE3 was measured in both solvent mixtures. A clear peak in the conductance histogram (without data

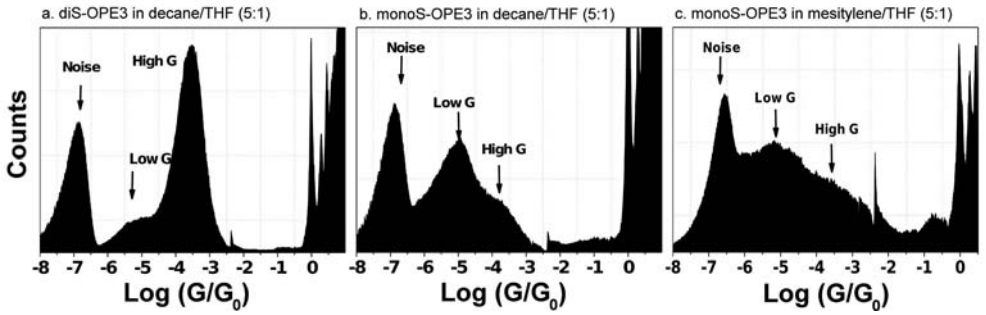

Figure 7.9 Histograms from all conductance-distance traces measured in STM break junctions at a bias of 100 mV for **a. diS-OPE3**, dissolved in decane/THF (5:1), **b. monoS-OPE3**, dissolved in decane/THF (5:1), and **c. monoS-OPE3**, dissolved in mesitylene/THF (5:1). (*Bern,* note 25)

selection) was obtained in decane/THF (Figure 7.9b), whereas the features in the histogram from the measurements in mesitylene/THF are much broader (Figure 7.9c). Similar trends were found for the monoS-analogues of naphthalene wire 4.4 and anthracene wire 4.5.[12] This is a compelling indication for enhanced π-π stacking in the junctions in decane, as predicted.

The strong conductance peak in the histogram of **monoS-OPE3** measured in decane is located at 10^{-5} G_0 (~0.8 nS), which is close to the previously reported values. This value is very close to the G2 (or: Low G) value of **diS-OPE3**, which we attributed to a different contact geometry. Hence, although the arguments for a low conductance signal due to an adatom-top or adatom-adatom configuration as presented in Chapter 4.7 are also strong, we cannot exclude a contribution of π-π stacking to this peak.[27]

We note that the formation of junctions upon π-π stacking of monothiolated π-conjugated wires is more likely to happen in the presence of a solution of these monothiols (as in the STM-BJ experiments) than in a junction in vacuum, where less molecules are present on the gold surface (Section 7.2.2). In such a junction in vacuum, the chance to observe a conductance signal from π-π stacked monothiols is strongly influenced by the number of molecules absorbed on the junction and their distance from the exact position where the Au-Au junction breaks, which could vary from experiment to experiment. From the 2D histogram shown in Figure 7.7 we cannot conclude that the formation of junctions by π-π stacked monothiols is impossible in MCBJs in vacuum, however in this experiment no peaks or plateaus due to π-π stacking were observed.

7.3 Perspectives of Molecular Electronics and π-Logic

Having investigated and discussed how both the structure of molecules and the junction geometry influence molecular conductance, we conclude this thesis with a discussion regarding the consequences of these results on the perspectives of molecular circuits and π-logic[30] (see Chapter 1.3). Even though the field of molecular electronics has expanded tremendously during the past five to ten years, as have the experimental possibilities, contacting molecules selectively with more than two electrodes (as required for π-logic) is a remaining challenge. Constructing electronic circuits from molecules only has still a long way to go. Since the understanding of molecular electronics has increased, we will evaluate our results on π-conjugated molecules from a more fundamental perspective.

The results presented in this thesis are mainly grouped in two categories: linear conjugated molecular wires (Figure 7.10a) and π-conjugated wires with an alternative conjugation pattern (*i.e.*, cross-conjugation and broken conjugation). Figure 7.10b shows the cross-conjugated anthraquinone-based wire, which has the potential to switch to a linear conjugated state, as described in Chapter 2. We note that this anthraquinone wire is doubly cross-conjugated: the bold pathway in Figure 7.10b has three subsequent single bonds and alternative pathways through this molecule for instance include two times two subsequent single bonds. We assume this double cross-conjugation not to influence our conclusions when comparing linear conjugated and cross-conjugated molecular wires.

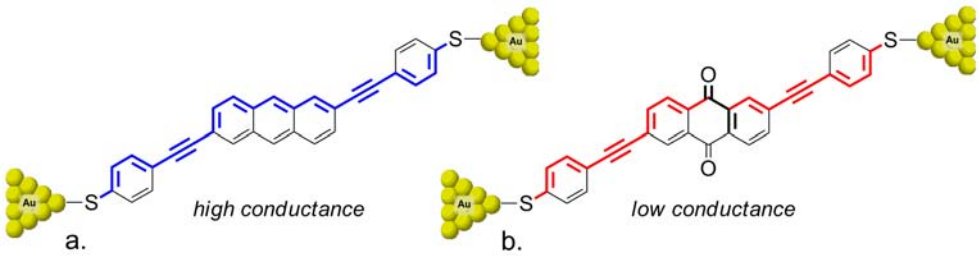

Figure 7.10 Schematic of the linear conjugated anthracene wire (**a.**) and the cross-conjugated anthraquinone wire (**b.**) attached to gold electrodes.

Linear Conjugated Molecular Wires

We found that the molecular conductance of linear conjugated molecules is mainly determined by their length. The only thing that distinguishes linear conjugated molecules from alkanethiols is that their length dependence is less strong (lower β values). Properties such as the energetic position of the HOMO level and the HOMO-LUMO gap have only a relatively minor influence on the conductance. However, here we should comment that these conductance studies mainly consider the low bias conductance (~100 mV), where at higher voltages the conductance of π-conjugated molecular wires increases significantly.[31] Charge transport through the discussed electrode-molecule-electrode junctions is best described as non-resonant tunneling. However, a transition from tunneling to a hopping mechanism has been reported for longer π-conjugated molecules (~4 nm for oligoarylene-imides[32] and ~2.5 nm for OPEs[33]). The decrease of the conductance with length is less strong (linear instead of exponential) when the hopping mechanism takes over, though the absolute conductance values are lower compared to tunneling. Further influences of molecular structure on hopping-dominated transport through longer molecular wires are to be explored.

Cross-conjugated Molecular Wires

We have investigated the influence of the conjugation pattern on the molecular conductance by comparing the molecules depicted in Figure 7.10 and found support for the assumption made in the development of the π-logic concept[30] that the cross-conjugated molecule has a about fifty times lower conductance than the linear conjugated molecule (of nearly identical length). This difference is better explained by quantum interference effects of the wave functions of transmitted electrons than by hindered delocalization of charges in cross-conjugated pathways (for in a real non-resonant tunneling model, no charges reside on the molecule in the tunnel junction). Quantum interference effects are generally found around the Fermi energy for cross-conjugated molecules,[34,35] resulting in lower conductances. However, they are not necessarily limited to this class of compounds and have also been predicted for linear conjugated molecules with nitro-substituents,[36,37] with alkene substituents,[38] and for molecules with fluorenone and related groups incorporated.[39] Quantum interference has the potential to tune the conductance over several orders of magnitude, making it highly suitable for conductance switching, and ultimately, chemical computing. Although we found strong indications for quantum interference in our experimental results, experimental

proof for quantum interference is still to be observed.

In the molecules that were designed as logic gates in the π-logic concept (Chapter 1.3), the conjugation pattern of pathways between terminals was compared instead of the conjugation pattern of rod-shaped wires (Chapter 5). In these larger π-conjugated structures, all possible pathways between the terminals can be considered as transmission channels for the conductance. During the development of π-logic, linear conjugated pathways were considered to have a transmission of "1" and cross-conjugated pathways to have "0" transmission. However, the (only available) linear conjugated pathway is often much longer than the shortest cross-conjugated pathway. When the transmission through this (short) cross-conjugated pathway is reduced seriously by quantum interference, its conductance will be dominated by the σ-system.[40] It is unlikely that the transmission through a short σ-pathway is indeed "0" compared to the transmission through significantly longer linear conjugated pathway, since the difference in conductance for molecules of (nearly) identical length was only about two orders of magnitude. Transport calculations would give more insights into the perspectives of π-logic.

7.4 References and Notes

1. CP-AFM measurements were performed by Constant Guédon and Sense Jan van der Molen at Leiden Univerity.
2. S. Creager, C.J. Yu, C. Bamdad, S. O'Connor, T. MacLean, E. Lam, Y. Chong, G.T. Olsen, J. Luo, M. Gozin, J.F. Kayyem, *J. Am. Chem. Soc.* **1999**, *121*, 1059-1064.
3. K. Liu, G. Li, X. Wang, F. Wang, *J. Phys. Chem. C* **2008**, *112*, 4342-4349.
4. Q. Lu, K. Liu, H. Zhang, Z. Du, X. Wang, F. Wang, *ACS Nano* **2009**, *3*, 3861-3868.
5. Ambient MCBJ measurements were performed by Wenjing Hong, in the group of Thomas Wandlowski at the Univerity of Bern.
6. E. Lörtscher, H.B. Weber, H. Riel, *Phys. Rev. Lett.* **2007**, *98*, 176807.
7. A. Salomon, D. Cahen, S. Lindsay, J. Tomfohr, V.B. Engelkes, C.D. Frisbie, *Adv. Mater.* **2003**, *15*, 1881-1890.
8. Yang, Y. Qian, C. Engtrakul, L. Sita, G. Liu, *J.Phys.Chem.B* **2000**, *104*, 9059-9062.
9. D. Nilsson, S. Watcharinyanon, M. Eng, L. Li, E. Moons, L.S.O. Johansson, M. Zharnikov, A. Shaporenko, B. Albinsson, J. Martensson, *Langmuir* **2007**, *23*, 6170-6181.
10. P.A. van Hal, E.C.P. Smits, T.C.T. Geuns, H.B. Akkerman, B.C. de Brito, S. Perissinotto, G. Lanzani, A.J. Kronemeijer, V. Geskin, J. Cornil, P.W.M. Blom, B. de Boer, D.M. de Leeuw, *Nat. Nanotechnol.* **2008**, *3*, 749-754.
11. E.A. Weiss, R.C. Chiechi, G.K. Kaufman, J.K. Kriebel, Z. Li, M. Duati, M.A. Rampi, G.M. Whitesides, *J. Am. Chem. Soc.* **2007**, *129*, 4336-4349.
12. All junctions shorted when triethylamine was omitted from the solutions used for the formation of the SAMs.
13. H.B. Akkerman, B. de Boer, *J. Phys.: Condens. Matter* **2008**, *20*, 013001.
14. J.R. Quinn, F.W. Foss, L. Venkataraman, R. Breslow, *J. Am. Chem. Soc.* **2007**, *129*, 12376-12377.
15. R. Breslow, F.W. Foss, *J. Phys.: Condens. Matter* **2008**, *20*, 374104.
16. A.M. Fraind, J.D. Tovar, *J. Phys. Chem. B* **2010**, *114*, 3104-3116.
17. H. Skulason, C.D. Frisbie, *J. Am. Chem. Soc.* **2000**, *122*, 9750-9760.
18. UHV MCBJ measurements were performed by Christian Martin and Roel Smit in the groups of prof. Herre van der Zant at Delft University of Technology and prof. Jan van Ruitenbeek at Leiden University.
19. C.A. Martin, R.H.M. Smit, R. van Egmond, H.S.J. van der Zant, J.M. van Ruitenbeek, *manuscript in preparation*; R.H.M. Smit *et al.*, *manuscript in preparation.*
20. X. Xiao, L.A. Nagahara, A.M. Rawlett, N. Tao, *J. Am. Chem. Soc.* **2005**, *127*, 9235-9240.
21. R. Huber, M.T. Gonzalez, S. Wu, M. Langer, S. Grunder, V. Horhoiu, M. Mayor, M. Bryce, C. Wang, R. Jitchati, C. Schönenberger, M. Calame, *J. Am. Chem. Soc.* **2008**, *130*, 1080-1084.
22. Y. Xing, T. Park, R. Venkatramani, S. Keinan, D.N. Beratan, M.J. Therien, E. Borguet, *J. Am. Chem. Soc.* **2010**, *132*, 7946-7956.
23. K. Liu, X. Wang, F. Wang, *ACS Nano* **2008**, *2*, 2315-2323.

24. C.A. Martin, D. Ding, J.K. Sørensen, T. Bjørnholm, J.M. van Ruitenbeek, H.S.J. van der Zant, *J. Am. Chem. Soc.* **2008**, *130*, 13198-13199.

25. STM-BJ measurements were performed by Bhadra Kaliginedi, in the group of Thomas Wandlowski at the Univerity of Bern.

26. S. Wu, M.T. González, R. Huber, S. Grunder, M. Mayor, C. Schönenberger, M. Calame, *Nat. Nanotechnol.* **2008**, *3*, 569-574.

27. S. Martín, I. Grace, M.R. Bryce, C. Wang, R. Jitchati, A.S. Batsanov, S.J. Higgins, C.J. Lambert, R.J. Nichols, *J. Am. Chem. Soc.* **2010**, *132*, 9157-9164.

28. C.A. Hunter, K.R. Lawson, J. Perkins, C.J. Urch, *J. Chem. Soc., Perkin Trans. 2* **2001**, 651-669.

29. D.S. Seferos, S.A. Trammell, G.C. Bazan, J.G. Kushmerick, *PNAS* **2005**, *102*, 8821-8825; D.S. Seferos, A.S. Blum, J.G. Kushmerick, G.C. Bazan, *J. Am. Chem. Soc.* **2006**, *128*, 11260-11267.

30. M. H. van der Veen, *PhD Thesis* "π-Logic" *University of Groningen*, **2006**.

31. E. Lörtscher, M. Elbing, M. Tschudy, C. von Hänisch, H.B. Weber, M. Mayor, H. Riel, *ChemPhysChem* **2008**, *9*, 2252-2258.

32. S.H. Choi, B. Kim, C.D. Frisbie, *Science* **2008**, *320*, 1482-1486; S.H. Choi, C. Risko, M.C.R. Delgado, B. Kim, J. Brédas, C.D. Frisbie, *J. Am. Chem. Soc.* **2010**, *132*, 4358-4368.

33. Q. Lu, K. Liu, H. Zhang, Z. Du, X. Wang, F. Wang, *ACS Nano* **2009**, *3*, 3861-3868.

34. D.Q. Andrews, G.C. Solomon, R.H. Goldsmith, T. Hansen, M.R. Wasielewski, R.P. Van Duyne, M.A. Ratner, *J. Phys. Chem. C* **2008**, *112*, 16991-16998.

35. T. Markussen, R. Stadler, K.S. Thygesen, *Nano Lett.* **2010**, *10*, 4260-4265.

36. N. Renaud, M. Ito, W. Shangguan, M. Saeys, M. Hliwa, C. Joachim, *Chem. Phys. Lett.* **2009**, *472*, 74-79.

37. R. Stadler, *Phys. Rev. B* **2009**, *80*, 125401.

38. M. Ernzerhof, M. Zhuang, P. Rocheleau, *J. Chem. Phys.* **2005**, *123*, 134704.

39. T.A. Papadopoulos, I.M. Grace, C.J. Lambert, *Phys. Rev. B* **2006**, *74*, 193306; C. Wang, M.R. Bryce, J. Gigon, G.J. Ashwell, I. Grace, C.J. Lambert, *J. Org. Chem.* **2008**, *73*, 4810-4818.

40. G.C. Solomon, D.Q. Andrews, R.H. Goldsmith, T. Hansen, M.R. Wasielewski, R.P. Van Duyne, M.A. Ratner, *J. Am. Chem. Soc.* **2008**, *130*, 17301-17308.

Publications

Synthesis and Properties of an Anthraquinone-Based Redox Switch for Molecular Electronics
E. H. van Dijk, D. J. T. Myles, M. H. van der Veen, J. C. Hummelen, *Org. Lett.* **2006**, *8*, 2333-2336.

Foldamers at Interfaces
J. van Esch, H. Valkenier, S. Hartwig, S. Hecht, *Foldamers: Structure, Properties, and Applications* (Eds.: S. Hecht, I. Huc), Wiley-VCH, Weinheim, **2007**, 403-426.

Using bis(pinacolato)diboron to improve the quality of regioregular conjugated co-polymers
F. Brouwer, J. Alma, H. Valkenier, T. P. Voortman, J. Hillebrand, R. C. Chiechi, J. C. Hummelen, *J. Mater. Chem.* **2011**, *21*, 1582-1592.

Controlling the interparticle distance in a 2D molecule-nanoparticle network
C. M. Guédon, J. Zonneveld, H. Valkenier, J. C. Hummelen, S. J. van der Molen, *Nanotechnology*, **2011**, *22*, 125205.

The Formation of High Quality Self-Assembled Monolayers of Conjugated Dithiols on Gold: Base Matters
H. Valkenier, E. H. Huisman, P. A. van Hal, D. M. de Leeuw, R. C. Chiechi, J. C. Hummelen, *J. Am. Chem. Soc.* **2011**, *133*, 4930-4939.

Effect of molecular length and molecular structure on the conductance of OPE type molecular wires: An STM break junction approach
V. Kaliginedi, H. Valkenier, V. M. García-Suárez, P. Moreno-García, W. Hong, P. Buiter, J. L. H. Otten, J. C. Hummelen, C. Lambert, Th. Wandlowski, *manuscript in preparation*.

Evidence for Quantum Interference in SAMs of Arylethynylene Thiolates in Tunneling Junctions with Eutectic Ga-In (EGaIn) Top-Contacts
D. Fracasso, H. Valkenier, J. C. Hummelen, G. Solomon, R. C. Chiechi, *J. Am. Chem. Soc.* **2011**, *in press.*

Observation of Quantum Interference in Molecular Charge Transport
C. M. Guédon, H. Valkenier, T. Markussen, K. S. Thygesen, J. C. Hummelen, S. J. van der Molen, *submitted.*

The influence of the conjugation pattern on charge transport in Au-molecule-Au junctions
H. Valkenier, C. M. Guédon, T. Markussen, K. S. Thygesen, S. J. van der Molen, J. C. Hummelen, *manuscript in preparation.*